Characterization of the *halved undersquinted scarf* carpentry connection.

Perria Elena
Università di Firenze, DICEA, Firenze, Italy
Technische Universität Braunschweig, iBHolz, Braunschweig, Germany

Paradiso Michele
Università di Firenze, DIDA, Firenze, Italy

Kessel Martin
Technische Universität Braunschweig, iBHolz, Braunschweig, Germany

ABSTRACT: The *halved undersquinted scarf* is a peculiar carpentry connection used in timber frame structures and roofs. In the classical engineering analysis, this kind of connections are usually described as hinges, able to transfer axial load but without any bending load bearing capacity. Nevertheless, from the observation and analysis of existing structures it is clear that, due to the shrinkage of the wood, wrong montage or imperfections in the structure, the connection is usually in the condition to bear eccentric forces. In the paper, a static model for the description of the behaviour of the connection is presented. Furthermore, the results of the experimental campaigns are illustrated. The work has been developed with the continuous validation of the analytic model on the base of the experimental results. Different aspects that influence the behaviour of the connection loaded in pure compression, pure bending and combined compressive and bending force are analysed. The description of carpentry connections through a static model is of importance in a scientific field for the knowledge of the mechanical behaviour of old constructional systems and many applications in the structural analysis with the aim of reinforce and restoration of old timber structures.

1 INTRODUCTION

The description of a structure through a static model is of importance in a scientific field, for many applications in the structural analysis. Nevertheless, *the analysis of structures shall be carried out using static models which consider to an acceptable level of accuracy the behaviour of the structure and of the supports* [3]. To properly understand the behaviour of old timber frames, the understanding of the influence of the connections is of importance. The main factors to be taken into account for the study of the mechanical behaviour of the carpentry joints are:

- the stiffness and strength of the joints depends on the material orthotropic properties and on the loading conditions;
- the static indetermination of the old timber structures. The loads can in fact follow different pathways and that means, solve additional equations to express the relative stiffness of all those pathways;

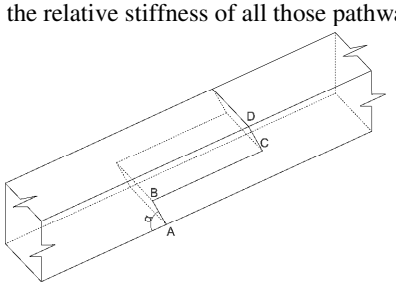

Figure 1. *Halved and undersquinted scarf* joint.

- the non-linearity of the geometry during the loading process;
- the imperfections of both the structure and the joints bring to an irregular and eccentric distribution of the forces;
- the transferring of forces among the members via contact pressure or friction of the facing surfaces. [2]

1.1 *Objectives*

The present study examines in detail the behaviour of the *halved undersquinted scarf* stressed by pure compression, pure bending and combined compressive and bending load. The N-M interaction diagrams for each of the loading conditions and geometries are proposed.

1.2 *Geometric description and diffusion*

The *halved and undersquinted scarf joint* (Figure 1), together with the simpler *halved scarf* version is one of the most common among the lengthening joints, and more specifically among the *Scarf joints*, a peculiar carpentry connection used in timber frame structures and roofs for the elongation of timber elements. *Halved* refers to the cut of the horizontal surface, that is in correspondence of the half of the timber cross section. *Undersquinted* refers to the angle for the squints that is considered equal to an angle α.

The simplest version of the *halved joint* is characterized by the inclination of the abutments α=90°. The *halved and undersquinted scarf joint* is, in respect to the simply *halved*, improved for the bending strength and resistance to seasoning twist thanks to the inclination of the squints. The joint is able to resist mainly the axial compression. It has moderate shear strength and bending capacity depending on the angle of the abutment: the shallower the angle, the easier the notch is subject to the shear/tension failure; for bigger angles, the same failure mode is reached with a higher level of load.

Some of these joints are provided with pins, nails or screws that are inserted to absorb shear force in case of external torsion or tension stress. The present study disregards the effectiveness of the *half splayed scarf* depending on these elements, considered as reinforcements, and focuses on load-transmission mechanism among the members via contact pressure and friction.

1.3 *State-of-the-art*

In the classical engineering analysis, this kind of connections are usually described as hinges, able to transfer axial load but without any bending load bearing capacity. They are classically calculated as stressed in pure tension/compression as the member they belong to. Nevertheless, from the observation and analysis of existing structures it is clear that due to the shrinkage of the wood, wrong assembly or imperfections in the structure, the connection is usually in the condition to bear eccentric forces, that means they show a semi-rigid behavior. According with [5], the *fictitious beam elements and spring elements may be used to model eccentric connections. The orientation of fictitious beam elements and the location of the spring elements should coincide as closely as possible with the actual joint configuration.* Both the axial and rotational stiffness are parameters that have to be considered for the evaluation of the joint. The value of *rotational stiffness k* for the spring in the hinge, defines a better qualification of the rigid or flexible behaviour of the member through the equation

$$\alpha=kL/EI \tag{1}$$

The relation that connect the moment and rotation, through the parameter *k* is:

$$M = K \cdot \theta \tag{2}$$

The rotational stiffness in the *halved and undersquinted scarf joint* is a parameter related to the geometry, as the squint angle, the joint length, the splay of the central surface and the friction between the facing surfaces. With the purpose of a good understanding of how the joint works and how the loads are balanced, all those parameters, together with the loading conditions and internal resulting forces, are estimated with static analysis, numerical modelling, and tests.

2 THE *HALVED UNDERSQUINTED SCARF JOINT – TESTS AND MODELS*

2.1 *Material and methods*

The general adopted methodology is generically the scientific method, consisting in the formulation of theories, and the systematic testing, measurement, observation, and modification of the initially adopted hypotheses. The initial formulation of a static model of the object of the research, based on a previous experimental observation of the behaviour of the connection, it is constantly verified by means of experimental tests and measurements. The continuous comparison between the analytical model and the experimental evidence, allowed the adjustment of the simplified static model to the complexity of reality, and guarantees the feasibility of the proposed models. All the calculations and tests are performed in accordance with the Eurocode 5 regulations.

2.2 *The models*

From the observations done during the first test was noticed that during the loading process, the contact surfaces (whole depth of the cross-section of the beam) along the segments AB (surface2), BC (surface1) and CD (surface3), are observed reducing in the direction of the beam's axis, in dependence of the applied load. This behaviour, observed during the loading process, brings to a progressive change of the distribution of the forces along these surfaces, and, as a consequence, a variation of the position of the internal resultant forces. The passage from the zero load to the ultimate-load shows a non-linear-geometric behaviour, and should be described through a non-linear-geometric model; however, that non-linear behaviour can be simplified in a sequence of static models, where in different loading-instants the position of such resultant forces is described through proper parameters. The sequence of equilibrium configurations under the loading conditions M, M+N, N, are described by different interactions and values of the internal resultant forces $F_{1,\perp}$, $F_{2,\perp}$ and $F_{3,\perp}$, respectively described by the parameters ε_1, ε_2, ε_3. The position of the external force F, independent from the axial applied moment M, is defined through the parameter e_F. A more exhaustive description of these parameters follows.

The basic hypothesis for the development of that work are:

- Hp. 1: The presence of only compressive force in the contact surfaces (no tension force is allowed);
- Hp. 2: The absence/presence of the friction force in the contact surfaces (in dependence of the proposed static model);

• Hp. 3: The perfect matching of the contact areas of the two facing surfaces (no gaps or imperfections in the connection).

2.3 *The parameters: ε_1, ε_2, ε_3 and ε_F*

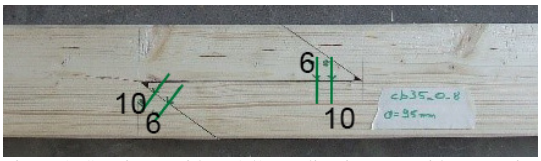

Figure 2. Specimen with α=35° Loading in F+M with eccentricity of the load e_F =95 mm (M=F·e_F).

In the Figure 2 is shown the non-linearity of the geometry along the loading process, as discussed in the paragraph 2. The position of the respective resultant force $F_{\perp}$ at the time of loading F is represented with a green line. For example, the point 6 on the surface AB represents the position of $F_{2,\perp}$ when the load is F=6kN (M=6·95 kNmm); the same is valid for the point 10.

The parameters ε_i describe the position of the correspondent internal force as following described. The parameter ε_1 defines, the position of the resultant force $F_{1,\perp}$:

$$e_1 = \varepsilon_1 \cdot l_{BC} \qquad 0 \le \varepsilon_1 \le 1 \qquad (4)$$

The parameter ε_2 defines, the position of the resultant force $F_{2,\perp}$:

$$e_2 = \varepsilon_2 \cdot l_{AB} \qquad 1 \le \varepsilon_2 < 0 \qquad (5)$$

The parameter ε_3 defines, the position of the resultant force $F_{3,\perp}$:

$$e_3 = (1-\varepsilon_2) \cdot l_{AB} \qquad 0 < \varepsilon_3 \le 1 \qquad (6)$$

Based on observations effectuate during the tests, the basic configuration correspondent to the zero-load is $\varepsilon_1 = 1/2$, $\varepsilon_2 = 1/2$ and $\varepsilon_3 = 1/2$.

The parameter ε_F describes the position of the applied force F. That parameter refers to the height of the cross section and it is defined as follows:

$$e_F = \varepsilon_F \frac{h}{2} \qquad -\infty < \varepsilon_F < +\infty \qquad (7)$$

The e_F is null in correspondence with the axis of the beam. For the present work, the force F is applied on the beam's axis; therefore, $\varepsilon_F = 0$.

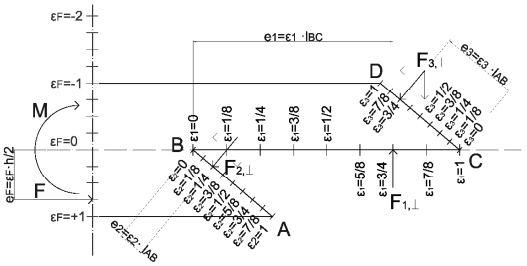

Figure 3. Parameters ε_1, ε_2, ε_3 and ε_F

2.4 *The analytic models (ii) and (vii)*

In the present section, the two analytic models are described.

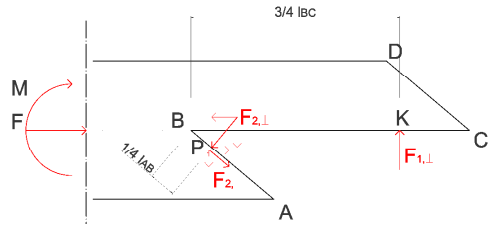

Figure 4. Equilibrium configuration (ii).

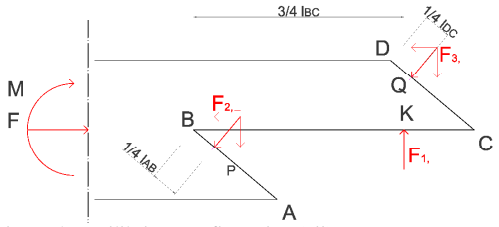

Figure 5. Equilibrium configuration (vii).

The model (ii) (Figure 4) describes the configuration with the generic angle α, where the influence of the static friction μ_α on the surface AB, influent for the earlier stages of the loading process (small F and small M), is considered. From the HP1 the condition

FC(ii)1.2: $F_{1,\perp} > 0$ (8)

that satisfy the Hp.1 for the surface BC, and the limit state LS3:

$$F_{1,\perp} = F \frac{\cos\alpha + \mu_\alpha \sin\alpha}{\sin\alpha - \mu_\alpha \cos\alpha} \le F_f \qquad (9)$$

F_f is the ultimate load [5], [6]. The friction coefficient results:

$$-\frac{1}{\tan\alpha} \le \mu_\alpha < \tan\alpha \qquad (10)$$

During the performed test was noticed that with the increasing of the load F the $F_{3,\perp}$ is "activated". The model (vii) (Figure 5) describes such configuration, where the contribution of the friction force is negligible due to the "reinforcing effect" of the compression force.

3 EXPERIMENTAL VERIFICATION OF THE MODELS

3.1 *The tests*

The geometry adopted for the tests is the one illustrated in the Figure 6. The specimens were tested in pure bending, pure compression and combined compressive and bending load. The machine (Figure 7)

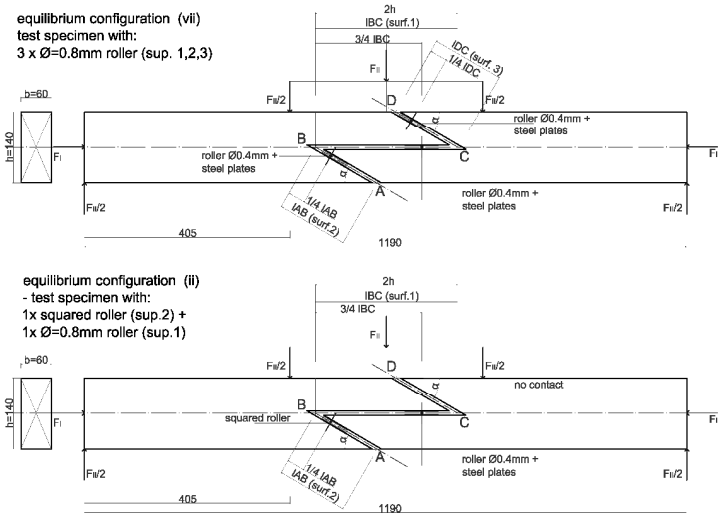

Figure 6. Load conditions and geometry of the specimen

was assembled in order to have contemporary response on the bending and/or normal force. Referring to Figure 6, the pure compression F_I is applied in correspondence of the barycenter of the cross section of the beam, in order to get normal force F_I=N along the beam axis. The bending stress M is generated through a four-point-bending test with the application of F_{II} on the horizontal piston. The correspondence between F_{II} and the moment M is:

$$M = \frac{F_{II}}{2} \cdot 405 = [kN \cdot mm] \tag{3}$$

The machine permits the contemporary lecture of the active application of force on the two pistons. An interesting phenomena, the *passive response*, was observed during the test and regards the record of a *passive* force $F_{passive}$ on the inactive piston. In fact, during the application of the load F_i from the active piston, the joint rotates; therefore, because of its geometry, the two connected elements separate one from the other, and both the far ends displace. This deformation provokes the *passive* $F_{passive}$ compression load on the non-active piston records.

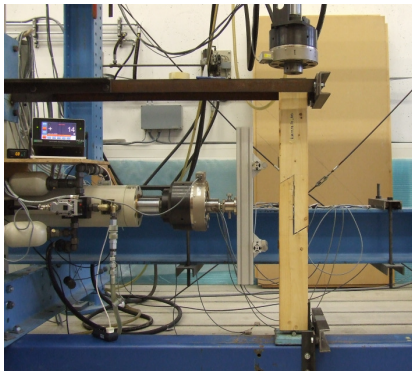

Figure 7. Test framework

In order to verify the conditions and the influence of the parameters described in the analytic model, for each of the static models an experimental verification for connections with squint α=30° and α=60° is proposed. The comparison among the real behavior and the static model behavior aims to evaluate the possible differences and fill the gap between the analytic and experimental results.

3.2 $e_{P,I}$ *(internal torque of equilibrium forces)*

The equation (11) describes the configuration where the direction of the vector-resultant-force $F_{1,\perp}$ is tangent to P, point of application of the resultant force $F_{2,\perp}$ and point of rotation for the equilibrium to the moment.

$$e_{1,P} = 2h\left(\varepsilon_1 - \frac{\varepsilon_2}{4\tan\alpha}\right) = 0 \tag{11}$$

that brings to the function

$$f(\varepsilon_1): \varepsilon_2 = \varepsilon_1 \cdot 4 \cdot \tan\alpha \tag{12}$$

represented in the Diagram 1. The observation, derived from both the analytic models (ii) and (vii), was demonstrated with tests. The alignment-configuration conf.1, conf.2 and conf.3 (Figure 8) were considered. For the model (ii) on the surface AB was used a device called *squared roller*, to

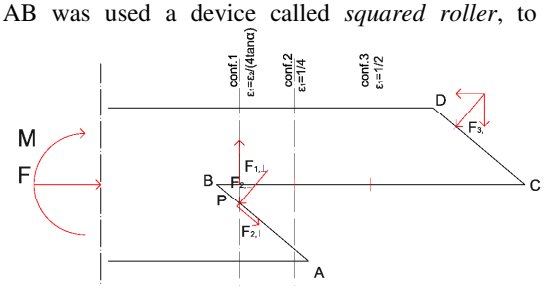

Figure 8. Configurations to demonstrate the GC1(ii) and (vii).

		α=30°			α=60°		
		M	M+F	M+FF	M	M+F	M+FF
		Model (ii)					
Conf.	1	kinematic	kinematic	-	kinematic	-	-
Conf.	2	equilibrium	equilibrium	-	kinematic	kinematic	equilibrium
Conf.	3	equilibrium	-	-	kinematic	equilibrium	equilibrium
		Model (vii)					
Conf.	1	kinematic	kinematic		kinematic	kinematic	
Conf.	2	kinematic	kinematic		kinematic	kinematic	
Conf.	3	kinematic	equilibrium	equilibrium	kinematic	kinematic	equilibrium

Figure 9. Equilibrium configurations – test results

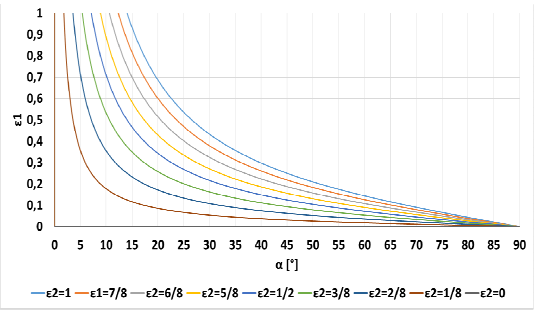

Diagram 1. GC1 – $e_{P,1}=0$ - $f(\varepsilon_1): \varepsilon_2 = \varepsilon_1 \cdot 4 \cdot \tan\alpha$

confer some amount of friction between the two facing surfaces; while, in the surface BC, in order to eliminate the friction component, a *circular roller* between two steel plates was employed (Figure 6). The rollers have the function to obligate the resultant force to the selected configuration. For the model (vii) In both the surfaces AB, BC and BC were used *circular rollers* between steel plates to eliminate the friction component. The specimen were manually loaded in pure bending M, in combined bending and compressive load (M+F) and more, with a bigger amount of compressive load summed up with bending (M+FF) for both =30° and α=60° (Figure 9).

In both the models the following observations on the positioning of the parameters were done:

a) The alignment-configurations (conf.1) always defines a kinematic configuration for the connection. This geometric boundary is independent from the external load conditions and model used.

b) Fixing ε_2, the load bearing capacity of the connection increases when the value of ε_1 increases.

c) Fixing ε_1, the load bearing capacity of the connection increases when the value of ε_2 decreases.

d) Considering both models and same configuration, the α=30° shows a bigger load bearing capacity respect to the α=60°.

e) Considering the same configuration and fixed M, for both models, is observed that with the increasing of the applied force F, the load bearing capacity of the connection increases.

3.3 *eP,3 (alignments of the centers in the model vii)*

For the model (vii) another interesting parameter to take into account is the alignment of the forces $F_{1,\perp}$ $F_{2,\perp}$ and $F_{3,\perp}$ (13, 14). In this case, the load-bearing capacity of the connection is also null, independently on the load conditions.

$$\begin{cases} e_{O,P} = 0 \\ e_{P,3} = 0 \end{cases} \tag{13}$$

$$\begin{cases} e_{O,P} = 2h\left(\varepsilon_1 \cdot \cos\alpha - \varepsilon_2 \dfrac{1}{4 \cdot \sin\alpha}\right) = 0 \\ e_{P,3} = 2h\left(\cos\alpha - \dfrac{\varepsilon_2 + \varepsilon_3}{4\sin\alpha}\right) = 0 \end{cases} \tag{14}$$

That gives as a solution (15).

$$\begin{cases} \varepsilon_3 = 2 \cdot (1 - \varepsilon_1) \cdot \sin(2\alpha) \\ \varepsilon_2 + \varepsilon_3 = 2 \cdot \sin(2\alpha) \end{cases} \tag{15}$$

following represented in the Diagram 2.

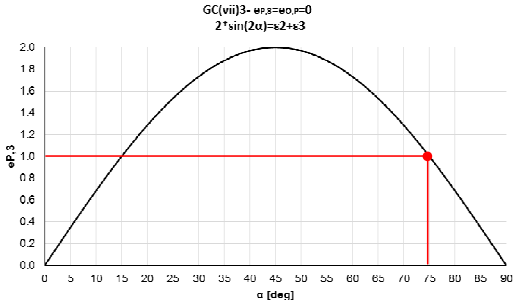

Diagram 2. $e_{P,3}=0$.

The following observations on the positioning of the parameters were done:

a) In case $e_{P,3} > 0$ the $F_{3,\perp}$ sum up with the external moment M (for small α).

b) The case where $e_{P,3} = 0$, the force $F_{3,\perp}$ has no counterpart in oppose the external applied moment M.

c) $e_{P,3} < 0$ the $F_{3,\perp}$ subtract the external moment M (for big α) and it contributes reducing the rotation of the connection caused by M.

For the demonstration of the hypothesis, a joint with squint α=75° (Figure 10) is considered. The rollers are set in correspondence of the positions ε_1=0.5, ε_2=0.5, ε_3=0.5 to satisfy (15) and the specimen is-manual loaded, first in pure bending and then in combined compression and bending force.

d) The joint failed under both loading conditions as hypothesized.

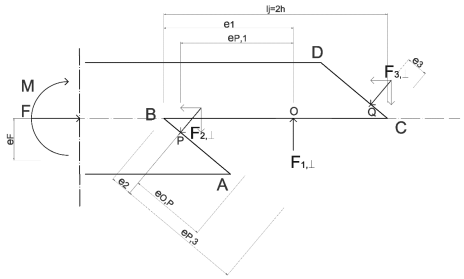

Figure 10. Parameter of calculation of the $e_{P,3}$=0.

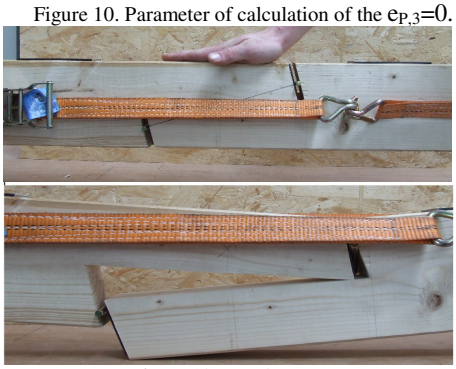

Figure 10. $e_{P,3}$=0 tests.

4 THE INFLUENCE OF THE NON LINEAR GEOMETRY

In order to explain the meaning of the parameters ε_1, ε_2, ε_3 and their definition in the static models, the tests following described were performed. For all the test specimen, the value of the parameters are:

(ii): ε1=variable, ε2=1/4; (16)

(vii): ε1=variable, ε2=1/4, ε3=3/4.

Key of the tests.:

Mod2_	30_	E1_	34_	F0/M0_	3_	k
model(ii)	α	ε1=	3/4	F_{II} load/ F_I load	specim. N°	contact

4.1 *F_{II} loading (F_I as response)*

In the Diagram 3 is represented the N-M equilibrium path defined by the specimens loaded with F_{II} (pure bending loading, $F_{I,\,passive}$ as a response).

In the Diagram 3, it is observed the following:

a) the load bearing capacity in pure bending increases when the position of the parameter ε_1 changes. This phenomenon is related with the non-linearity of the geometric parameters during the loading process. In fact, the configurations assumed by the joint during the loading process complies with the following order: at time equal to zero the joint assumes the position ε_1=1/4, then, with the increasing of the load F_{II}, the internal force $F_{1,\perp}$ assumes, first the configuration ε_1=1/2, and then the ε_1=3/4, until failure. Observing the test results, the specimen that have the configuration ε_1=3/4 are the ones that register the bigger bending capacity.

b) Furthermore, for the specimen Mod2_30_E1_F0_34_2and Mod2_30_E1_F0_34_3, is observed that the loading path remained on the line of F=0, pure bending, up to the loading value of M=130 kNmm. That means that until that point no passive response on the piston I was registered. With the further increasing of the bending force (F_{II}), the displacement of the connection, due to the deformation along the direction of the beam's axis, "activate" the compression on the piston I; there, the lecture on the $F_{I,passive}$ piston are increasing values. With the further increasing of the F_{II}, the F is increasing together with the M until failure.

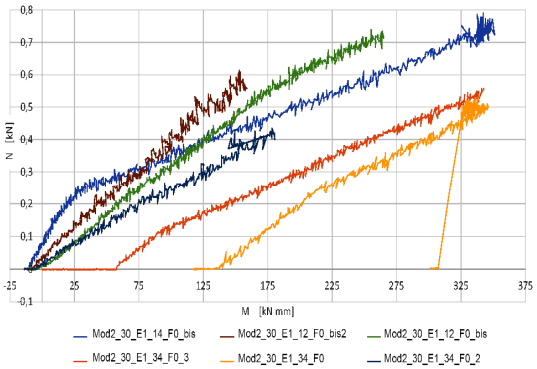

Diagram 3. Test results. Specimen loaded with F_{II}

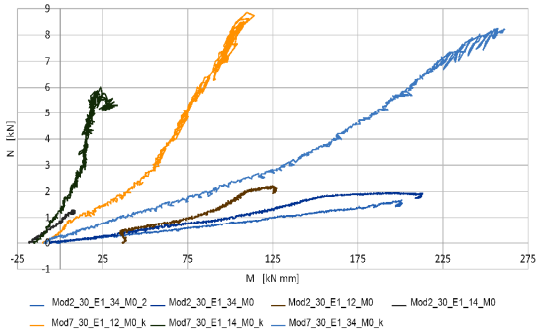

Diagram 4. Test result. Specimen loaded with F_I.

4.1 *F_I loading (F_{II} as response)*

The tests described in the Diagram 4 consist in the application of the F_I force from F_I and the $F_{I,passive}$ (M) as a response. The specimens named with letter k have contact on the surf.2 and surf.3 (vii) or the surf.2 (ii); the other specimens are assembled with rollers on both the surfaces 2 and 3 (vii) and on the surf. 2 (ii).

As demonstrated in the Diagram 3, the configuration ε_1=3/4 is the situation in which the connection

Commento [EP1]: Tabella modelli e forze??

reaches the maximum bending capacity; nevertheless, the load carrying capacity of the joint is not exhausted. A further increasing of the F_I is possible, but only with a reduction of the bending moment M, that brings to a new change of position of the ε_1. This conclusion is extrapolated from the Diagram 4 test results. Here, you may observe the different inclination of the three loading path for the different position of ε_1. For both the cases, with and without contact, the specimens ε_1=3/4 show higher moment capacity than the specimens ε_1=1/4 and ε_1=1/2; on the other side, the specimens ε_1=3/4 have lower normal force capacity respect to the specimens ε_1=1/4 and ε_1=1/2.

Is demonstrated that the configuration that permit the maximum amount of pure compression force F is either the configuration ε_1=1/4, or the ε_1=1/2; on the other side, the configuration that confers the maximum amount of moment resistance, is the ε_1=3/4.

Finally we can add that, apart from ε_1, also the parameters ε_2 (and ε_3 for (vii)) are geometric non-linear parameters. On the base of this same approach, was observed that the decreasing of the amount of ε_2, for same values of ε_3, the load carrying capacity in pure bending, increases the bending capacity of the joint. These latter results are generate from a more wide observation on the conducted experimental campaign that simulate the force position described by the analytical models. For editing reason, we cannot show all the results in detail.

5 CONCLUSIONS

- The load carrying capacity of a structure depends both on the material, the load-carry mechanism of the structure and the loads.
- The material wood does not guarantee the homogeneity of the results as it is an orthotropic material; for this reason, the experimental campaign was developed using artifices that simplify the understanding of the results.
- The main load carrying-mechanism of the connection is influenced by the geometry of the connection. The comparison between shallower and big angles give us the evidence of that statement.
- Not only the geometry of the connection, but also the configuration assumed by internal forces in the connection during the loading process is important; in fact, it confers it the characteristic load-bearing resistance. The tests demonstrate that, the configurations are variables and follow a specific path aimed to obtain the equilibrium of the connection until the failure.
- Finally, the load is an important factor to take into account for the prediction of the ultimate load and failure mode. The path followed by the specimens loaded in pure compression is very different from the one followed by the pure-compressed specimens, and both origin the other solicitation as an inducted force before reaching the failure.

The paper focus and refer only on some of the obtained results in the considered experimental campaign, where only on the *halved undersquinted scarf* with a squint inclined by α=30° is considered. Further test on α=60° have been developed and some other are planned in the recent future, in order to discuss the problem from a wider point of view.

6 AKNOWLEDGEMENTS

I thank the Labor für Holztechnik LHT in the HAWK Hildesheim and their technicians for their availability and punctuality in the execution of the tests.

7 BIBLIOGRAPHY

[1] Blass H.J. Aune P. et alii., *Timber Engineering, STEP 1, Basis of design, material properties , structural components and joints*, and *Timber Engineering, STEP 2, Design – Details and structural systems* Centrum Hout, Netherlands, 1995.

[2] Branco J. M., Descamps T., *Analysis and strengthening of carpentry joints* Construction and Building Materials, Special Issue: Reinforcement of Timber Structures. 97 (2015) 34–47.

[3] Eurocode 5, *Design of timber structures* - Part 1-1: General – Common rules and rules for buildings. EN 1995-1-1:2004.

[4] Fairham, William. *Woodwork joints; how they are set out, how made and where used; with four hundred and thirty illustrations and a complete index of eleven hundred references.* Philadelphia and London, J. B. Lippincott company, 1921

[5] Gustafsson, P. J., *A study of strength of notched beams*. In: Proc. of CIB-W18A Meeting 21, Parksville, Canada, 1988. Paper 21-10-1.

[6] Larsen, H. J. and Gustafsson, P. J., *The fracture energy of wood in tension perpendicular to the grain – results from a testing project*. In: Proc. Of CIB-W18A Meeting 23, Lisbon, Portugal, 1990. Paper 23-19-2.

[7] Madsen B., *Behaviour of Timber Connections*, 2000, Timber engineering Ltd., Vancouver, 2000.

[8] McGuire, J., (1995) "*Notes on Semi-Rigid Connections" Finite Element Modeling Continuous Improvement*.
http://femci.gsfc.nasa.gov/semirigid/index.html

[9] Sobon J.A. *Historic American timber joinery, a graphic guide.* Becket, MA 01223: Timber Framers Guild; 2012.